Li, Zhixiong; Ilyas Khan; Shafee, Ahmad; Tlili, I.; Asifa, T.

**Article**

# Energy transfer of Jeffery-Hamel nanofluid flow between non-parallel walls using Maxwell-Garnetts (MG) and Brinkman models

Energy Reports

**Provided in Cooperation with:**
Elsevier

*Suggested Citation:* Li, Zhixiong; Ilyas Khan; Shafee, Ahmad; Tlili, I.; Asifa, T. (2018) : Energy transfer of Jeffery-Hamel nanofluid flow between non-parallel walls using Maxwell-Garnetts (MG) and Brinkman models, Energy Reports, ISSN 2352-4847, Elsevier, Amsterdam, Vol. 4, pp. 393-399, https://doi.org/10.1016/j.egyr.2018.05.003

Energy Reports 4 (2018) 393–399

Contents lists available at ScienceDirect

Energy Reports

journal homepage: www.elsevier.com/locate/egyr

Research paper

# Energy transfer of Jeffery–Hamel nanofluid flow between non-parallel walls using Maxwell–Garnetts (MG) and Brinkman models

Zhixiong Li [b,c], Ilyas Khan [a,*], Ahmad Shafee [d], I. Tlili [e], T. Asifa [f]

[a] Faculty of Mathematics and Statistics, Ton Duc Thang University, Ho Chi Minh City, Viet Nam
[b] School of Engineering, Ocean University of China, Qingdao 266110, China
[c] School of Mechanical, Materials, Mechatronic and Biomedical Engineering, University of Wollongong, Wollongong, NSW 2522, Australia
[d] Public Authority of Applied Education & Training, College of Technological Studies, Applied Science Department, Shuwaikh, Kuwait
[e] Energy and Thermal Systems Laboratory, National Engineering School of Monastir, Street Ibn El Jazzar , 5019 Monastir, Tunisia
[f] College of Computer and Information Sciences, Majmaah University, Majmaah 11952, Saudi Arabia

ARTICLE INFO

*Article history:*
Received 17 April 2018
Received in revised form 14 May 2018
Accepted 20 May 2018

*Keywords:*
Energy transfer
Nanofluid
Galerkin method
Jeffery–Hamel flow

ABSTRACT

In this letter, energy transfer of Jeffery–Hamel nanofluid flow in non-parallel walls is investigated analytically using Galerkin method. The effective thermal conductivity and viscosity of nanofluid are calculated by the Maxwell–Garnetts (MG) and Brinkman models, respectively. The influence of the nanofluid volume friction, Reynolds number and angle of the channel on velocity and temperature profiles are investigated. Results show that Nusselt number increases with increase of Reynolds number and nanoparticle volume friction. Also it can be found that skin friction coefficient is an increasing function of Reynolds number, opening angle and nanoparticle volume friction.



## 1. Introduction

Nanotechnology suggests new kind of working fluid with higher thermal conductivity. Nanofluid can be used in various field of engineering. Fluid heating and cooling are important in many industries fields such as power, manufacturing and transportation. Effective cooling techniques are absolutely needed for cooling any sort of high energy device. Common heat transfer fluids such as water, ethylene glycol, and engine oil have limited heat transfer capabilities due to their low heat transfer properties. In contrast, metals thermal conductivities are up to three times higher than the fluids, so it is naturally desirable to combine the two substances to produce a heat transfer medium that behaves like a fluid, but has the thermal conductivity of a metal. Zin et al. (2017) investigated Jeffrey nanofluid free convection in a porous media under the effect of magnetic field. Abro and Khan (2017) investigated flow and heat transfer of Casson fluid in a porous medium. Sheikholeslami et al. (2018a) utilized nanoparticles for condensation process. They analyzed entropy generation and exergy loss of nano-refrigerant. Ullah et al. (2017) investigated slip effect on Casson fluid flow over a porous plate in existence of Lorentz forces. Sheikholeslami et al. (2018f) investigated exergy loss analysis for nanofluid forced convection heat transfer in a pipe with modified turbulators. Sheikholeslami et al. (2018d) presented nanofluid forced convection turbulent flow in a pipe. Sheikholeslami et al. (2018g) studied the nanofluid natural convection in a porous cubic cavity by means of Lattice Boltzmann method. Sheikholeslami (2018e) simulated solidification process of nano-enhanced PCM in a thermal energy storage.

There are some simple and accurate approximation techniques for solving differential equations called the Weighted Residuals Methods (WRMs). Collocation, Galerkin and Least Square are examples of the WRMs. Hosseini et al. (2018) utilized Galerkin method to investigated Nanofluid heat transfer analysis in a microchannel heat sink (MCHS) under the effect of magnetic field. Vaferi et al. (2012) have studied the feasibility of applying of Orthogonal Collocation method to solve diffusivity equation in the radial transient flow system. Hendi and Albugami (2010) used Collocation and Galerkin methods for solving Fredholm–Volterra integral equation. Recently Least square method is introduced by A. Aziz and M.N. Bouaziz (Bouaziz and Aziz, 2010) and is applied for a predicting the performance of a longitudinal fin Aziz and Bouaziz (2011). They found that least squares method is simple compared with other analytical methods. Shaoqin and Huoyuan (2008) developed and analyzed least-squares approximations for the incompressible magneto-hydrodynamic equations.

After introducing the problem of the flow of fluid through a divergent channel by Jeffery (Sheikholeslami et al., 2018f) and Hamel (1916) in 1915 and 1916, respectively, it is called Jeffery–Hamel flow. On the other hand, the term of Magneto hydro dynamic (MHD) was first introduced by Alfvén (Bansal, 1994) in 1970. The

* Corresponding author.
*E-mail address:* ilyaskhan@tdt.edu.vn (I. Khan).

https://doi.org/10.1016/j.egyr.2018.05.003

**Nomenclature**

| | |
|---|---|
| $A^*$ | Constant parameter |
| $B_0$ | Magnetic field(wb.m$^{-2}$) |
| $f(\eta)$ | Dimensionless velocity |
| Pressure term | Pressure term |
| $Re$ | Reynolds number |
| $r, \theta$ | Cylindrical coordinates |
| $U_{max}$ | Maximum value of velocity |
| $u, v$ | Velocity components along x, y axes, respectively |

**Greek symbols**

| | |
|---|---|
| $\alpha$ | Angle of the channel |
| $\eta$ | Dimensionless angle |
| $\theta$ | Any angle |
| $\rho$ | Density |
| $\phi$ | Nanoparticle volume fraction |
| $\mu$ | Dynamic viscosity |
| $\upsilon$ | Kinematic viscosity |

**Subscripts**

| | |
|---|---|
| $\infty$ | Condition at infinity |
| Nanofluid | $nf$ |
| Base fluid | $f$ |
| $s$ | Nano-solid-particles |

theory of Magneto hydro dynamics is inducing current in a moving conductive fluid in presence of magnetic field; such induced current results force on ions of the conductive fluid. The theoretical study of (MHD) channel has been a subject of great interest due to its extensive applications in designing cooling systems with liquid metals, MHD generators, accelerators, pumps and flow meters (Cha et al., 2002). In recent years, nanofluid has been used in various fields (Sheikholeslami and Shehzad, 2018a; Sheikholeslami et al., 2018b; Sheikholeslami and Rokni, 2018c, a; Sheikholeslami and Shehzad, 2018c; Chamkha et al., 2010; Mansour et al., 2010; Sheikholeslami and Seyednezhad, 2018; Sheikholeslami et al., 2018e; Sheikholeslami, 2018c, a; Chamkha and Ahmed, 2011; Raju and Sandeep, 2016; Sheikholeslami and Rokni, 2018b; Sheikholeslami, 2018b; Sheikholeslami and Shehzad, 2018b; Ali et al., 2016a, b, 2017; Imran et al., 2017; Jafaryar et al., 2018; Sheikholeslami, 2018d; Sheikholeslami et al., 2018c; Sheikholeslami and Sadoughi, 2018; Sheikholeslami and Rokni, 2017b; Fengrui et al., 2017a, b; Sheikholeslami and Seyednezhad, 2017a; Sheikholeslami et al., 2017; Sheikholeslami and Shehzad, 2017a; Sheikholeslami and Rokni, 2017c; Sheikholeslami, 2017c; Sheikholeslami and Shehzad, 2017b; Sheikholeslami and Sadoughi, 2017; Sheikholeslami and Zeeshan, 2017; Sheikholeslami, 2017b; Ahmed et al., 2017; Khan et al., 2017; Sheikholeslami and Bhatti, 2017; Sheikholeslami, 2017a; Sheikholeslami and Seyednezhad, 2017b; Shah et al., 2018; Sheikholeslami and Rokni, 2017a; Sheikholeslami and Ghasemi, 2018).

In this study, the purpose is to solve nonlinear equations through the GM. The effect of active parameters such as nanoparticle volume friction, opening angle and Reynolds number on velocity and temperature boundary layer thicknesses have been examined.

## 2. Problem description

Consider a system of cylindrical polar coordinates $(r, z, \theta)$ which steady two-dimensional flow of an incompressible conducting viscous fluid from a source or sink at channel walls lie in planes, and intersect in the axis of z. Assuming purely radial motion which means that there is no change in the flow parameter along the z direction. The flow depends on $r$ and $\theta$ (see Fig. 1).

The reduced forms of continuity, Navier–Stokes and energy equations are (Sheikholeslami et al., 2012):

$$\frac{\rho_{nf}}{r}\frac{\partial\,(ru(r,\theta))}{\partial r}(ru(r,\theta)) = 0, \tag{1}$$

$$u(r,\theta)\frac{\partial u(r,\theta)}{\partial r} = -\frac{1}{\rho_{nf}}\frac{\partial P}{\partial r} + \upsilon_{nf}\left[\frac{\partial^2 u(r,\theta)}{\partial r^2} + \frac{1}{r}\frac{\partial u(r,\theta)}{\partial r} + \frac{1}{r^2}\frac{\partial^2 u(r,\theta)}{\partial \theta^2} - \frac{u(r,\theta)}{r^2}\right], \tag{2}$$

$$\frac{1}{\rho_{nf} r}\frac{\partial P}{\partial \theta} - \frac{2\upsilon_{nf}}{r^2}\frac{\partial u(r,\theta)}{\partial \theta} = 0, \tag{3}$$

$$(\rho C_p)_{nf} u(r,\theta)\frac{\partial T(r,\theta)}{\partial r} = k_{nf}\left[\frac{1}{r}\frac{\partial}{\partial r}\left(r\frac{\partial T(r,\theta)}{\partial r}\right) + \frac{1}{r^2}\frac{\partial^2 T(r,\theta)}{\partial \theta^2}\right] + \mu_{nf}\left[2\left(\left(\frac{\partial u(r,\theta)}{\partial r}\right)^2 + \left(\frac{u(r,\theta)}{r}\right)^2\right) + \left(\frac{1}{r}\frac{\partial u(r,\theta)}{\partial r}\right)^2\right], \tag{4}$$

Where, $u_r$ is the velocity along radial direction, P is the fluid pressure, $\upsilon_{nf}$ the coefficient of kinematic viscosity and $\rho_{nf}$ the fluid density. The effective density $\rho_{nf}$, the effective dynamic viscosity $\mu_{nf}$ and kinematic viscosity $\upsilon_{nf}$ of the nanofluid are given as:

$$\rho_{nf} = \rho_f(1-\phi) + \rho_s\phi, \quad \mu_{nf} = \frac{\mu_f}{(1-\phi)^{2.5}}, \quad \upsilon_{nf} = \frac{\mu_f}{\rho_{nf}}, \quad \frac{k_{nf}}{k_f} = \frac{(k_s+2k_f) - 2\phi(k_s-k_f)}{(k_s+2k_f) + \phi(k_s-k_f)} \tag{5}$$

Here, $\phi$ is the solid volume fraction. Considering $u_\theta = 0$ for purely radial flow, one can define the velocity parameter as:

$$f(\theta) = ru_r \tag{6}$$

Introducing the $\eta = \frac{\theta}{\alpha}$ as the dimensionless degree, the dimensionless form of the velocity parameter can be obtained by dividing that to its maximum value as:

$$F(\eta) = \frac{f(\theta)}{u_c}, \frac{T}{T_w} = \frac{\Theta(\theta)}{r^2}, \eta = \frac{\theta}{\alpha}, \tag{7}$$

Substituting Eq. (6) into Eqs. (2) and (3), and eliminating P, one can obtain the ordinary differential equation for the normalized function profile as:

$$f'''(\eta) + 2\alpha\mathrm{Re}[(1-\phi) + \frac{\rho_s}{\rho_f}\phi] \times (1-\phi)^{2.5} f(\eta) f'(\eta) + 4\alpha^2 f'(\eta) = 0, \tag{8}$$

$$\Theta''(\eta) + 4\alpha^2\Theta(\eta) + \frac{(1-\phi) + \frac{(\rho c_p)_s}{(\rho c_p)_f}\phi}{\frac{(k_s+2k_f)-2\phi(k_s-k_f)}{(k_s+2k_f)+\phi(k_s-k_f)}} 2\alpha^2\,\mathrm{Pr} f(\eta)\Theta(\eta) + \frac{\mathrm{PrEc}}{\mathrm{Re}\frac{(k_s+2k_f)-2\phi(k_s-k_f)}{(k_s+2k_f)+\phi(k_s-k_f)}(1-\phi)^{2.5}}(4\alpha^2 f(\eta)^2 + f'(\eta)^2) = 0, \tag{9}$$

Where Re is Reynolds number, Pr is Prandtl number and Ec is the Eckert number. On introducing the following non-dimensional quantities,

$$\mathrm{Re} = \frac{f_{\max}\alpha}{\upsilon_f} = \frac{U_{\max} r\alpha}{\upsilon_f} \times \begin{pmatrix} divergent - channel : \alpha > 0, f_{\max} > 0 \\ convergent - channel : \alpha < 0, f_{\max} < 0 \end{pmatrix} \tag{10}$$

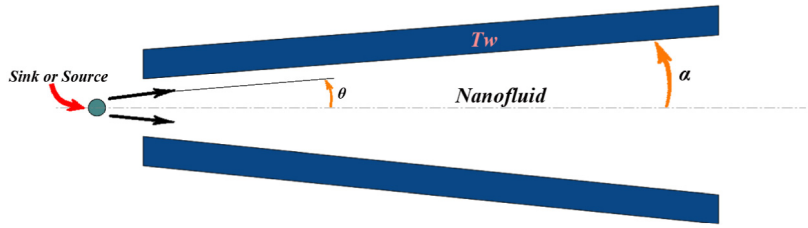


**Fig. 1.** Geometry of problem.

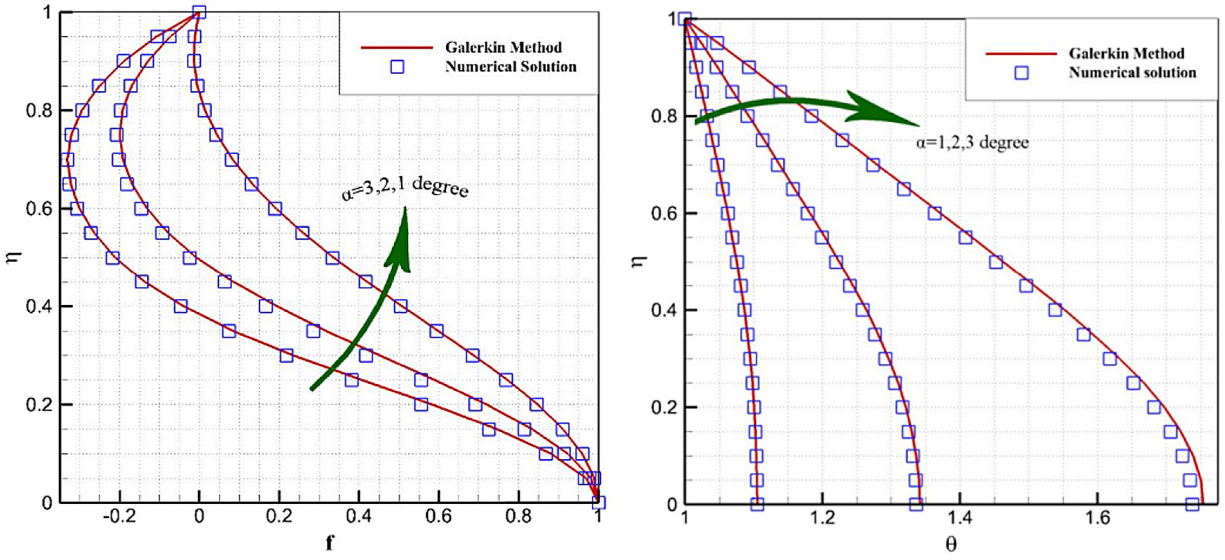


**Fig. 2.** Comparison between numerical and GM solution results.

$$\mathrm{Pr} = \frac{\alpha u_c^2}{c_{pf} T_w} \tag{11}$$

$$Ec = \frac{\alpha u_c^2}{c_{pf} T_w} \tag{12}$$

With the following reduced form of boundary conditions

$$\begin{aligned} &f(0) = 1, f'(0) = 0, f(\pm 1) = 0 \\ &\Theta(\pm 1) = 1, \Theta'(0) = 0 \end{aligned} \tag{13}$$

Physically these boundary conditions mean that maximum values of velocity are observed at centerline ($\eta = 0$) as shown in Fig. 1, and we consider fully develop velocity profile, thus rate of velocity is zero at ($\eta = 0$). Also, in fluid dynamics, the no-slip condition for fluid states that at a solid boundary, the fluid will have zero velocity relative to the boundary. The fluid velocity at all fluid–solid boundaries is equal to that of the solid boundary, so we can see that value of velocity is zero at ($\eta = 1$).

## 3. Weighted residual methods (WRMs)

There existed an approximation technique for solving differential equations called the Weighted Residual Methods (WRMs). Suppose a differential operator D is acted on a function $u$ to produce a function $p$:

$$D(u(x)) = p(x) \tag{14}$$

It is considered that $u$ is approximated by a function $\widetilde{u}$, which is a linear combination of basic functions chosen from a linearly independent set. That is,

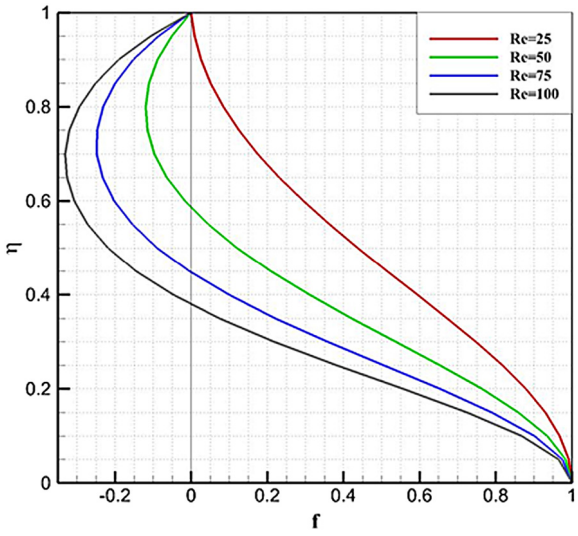


**Fig. 3.** Effect of the Reynolds number on the velocity profile $f(\eta)$versus $\eta$ when $\alpha = 3$, $Ec = 0.6$, $\phi = 0.04$ and $\mathrm{Pr} = 7$.

$$u \cong \widetilde{u} = \sum_{i=1}^{n} c_i \varphi_i \tag{15}$$

Now, when substituted into the differential operator, D, the result of the operations generally is not $p(x)$. Hence an error or

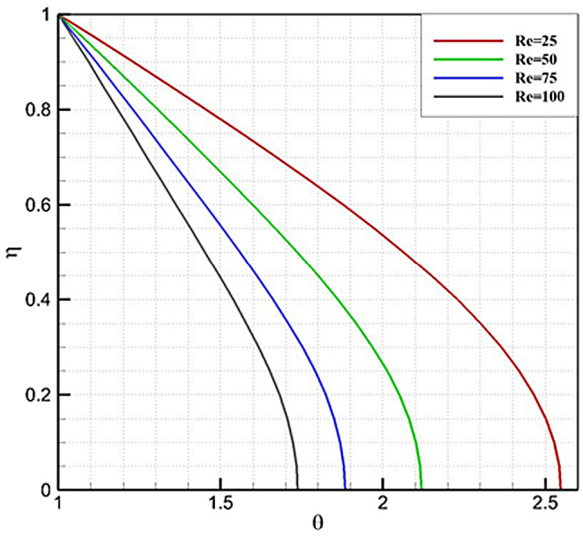


**Fig. 4.** Effect of the Reynolds number on the heat boundary layers profile. $\theta(\eta)$versus $\eta$ when$\alpha = 3$, $Ec = 0.6$, $\phi = 0.04$ and $\mathrm{Pr} = 7$.

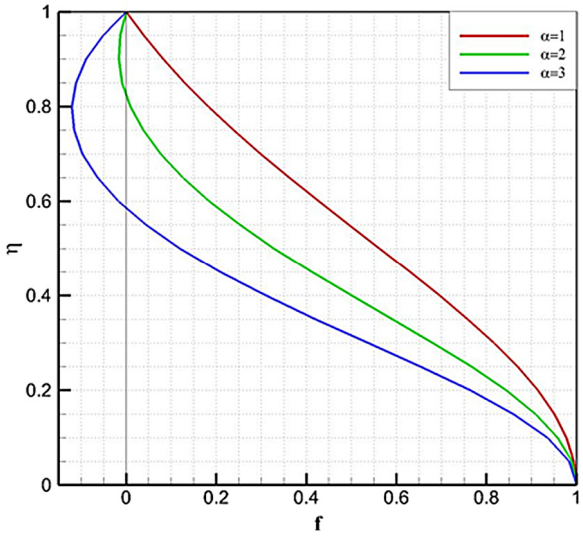


**Fig. 5.** Effect of the channel half angle on the velocity profile when $Re = 50$, $Ec = 0.6$, $\phi = 0.04$ and $\mathrm{Pr} = 7$.

residual will exist:

$$E(x) = R(x) = D(\widetilde{u}(x)) - P(x) \neq 0 \tag{16}$$

The notion in WRMs is to force the residual to zero in some average sense over the domain. That is:

$$\int_X R(x) W_i(x) = 0;\ i = 1, 2, \ldots, n \tag{17}$$

Where the number of weight functions Wi is exactly equal to the number of unknown constants *ci* in $\widetilde{u}$. The result is a set of n algebraic equations for the unknown constants ci. Two methods of WRMs are explained in the following subsections. Galerkin method may be viewed as a modification of the Least Square Method. Rather than using the derivative of the residual with respect to the unknown ci, the derivative of the approximating function or trial function is used. In this method weight functions are:

$$W_i = \frac{\partial \widetilde{u}}{c_i};\ i = 1, 2, \ldots, n \tag{18}$$

## 4. Solution with Galerkin method:

In this problem, the trial functions for two equations are considered as:

$$\begin{aligned} F(\eta) &= 1 - \eta^2 + c_1\left(\eta^2 - \eta^4\right) + c_2\left(\eta^2 - \eta^6\right) \\ &\quad + c_3\left(\eta^2 - \eta^8\right) + c_4\left(\eta^2 - \eta^{10}\right) + c_5\left(\eta^2 - \eta^{12}\right) \\ \theta(\eta) &= 1 + c_6(1 - \eta^2) + c_7(1 - \eta^4) \\ &\quad + c_8(1 - \eta^6) + c_9(1 - \eta^8) + c_{10}(1 - \eta^{10}) \end{aligned} \tag{19}$$

Now we apply GM for solving the F($\eta$) and $\theta(\eta)$ functions as non-dimensional velocities equation for nanofluid flow. First, as already were described, consider the trial functions as Eq. (14) which satisfies described boundary condition in Eq. (12). Using Eq. (17) weight functions will be obtained as:

$$\begin{aligned} &W_1 = \eta^2 - \eta^4, \quad W_2 = \eta^2 - \eta^6, \quad W_3 = \eta^2 - \eta^8, \\ &W_4 = \eta^2 - \eta^{10}, \quad W_5 = \eta^2 - \eta^{12} \\ &W_6 = 1 - \eta^2, \quad W_7 = 1 - \eta^4, \quad W_8 = 1 - \eta^6, \\ &W_9 = 1 - \eta^8, W_{10} = 1 - \eta^{10} \end{aligned} \tag{20}$$

and residual will be as,

$$\begin{aligned} &R(c_1, c_2, c_3, c_4, c_5, \eta) := -24c_1\eta - 120c_2\eta^3 - 336c_3\eta^5 \\ &\quad -720c_4\eta^7 - 1320c_5\eta^9 + \\ &2\mathrm{Re}\alpha(1-\phi)^{2.5}(1 - \phi + \frac{\rho_s}{\rho_f}\phi)(1 - \eta^2 + c_1(\eta^2 - \eta^4) \\ &\quad + c_2(\eta^2 - \eta^6) + c_3(\eta^2 - \eta^8) + c_4(\eta^2 - \eta^{10}) + \\ &c_5(\eta^2 - \eta^{12}))(-2\eta + c_1(2\eta - 4\eta^3) + c_2(2\eta - 6\eta^5) \\ &\quad + c_3(2\eta - 8\eta^7) + c_4(2\eta - 10\eta^9) + \\ &c_5(2\eta - 12\eta^{11})) + 4\alpha^2(-2\eta + c_1(2\eta - 4\eta^3) \\ &\quad + c_2(2\eta - 6\eta^5) + c_3(2\eta - 8\eta^7) + c_4(2\eta - 10\eta^9) + \\ &c_5(2\eta - 12\eta^{11})) \end{aligned}$$

$$\begin{aligned} &R(c_6, c_7, c_8, c_9, c_{10}, \eta) := -2c_6 - 12c_7\eta^2 - 30c_8\eta^4 \\ &\quad -56c_9\eta^6 - 90c_{10}\eta^8 + 4\alpha^2(1 + c_6(1 - \eta^2) + \\ &c_7(1 - \eta^4) + c_8(1 - \eta^6) + c_9(1 - \eta^8) + c_{10}(1 - \eta^{10})) \\ &\quad + \frac{2\alpha^2\,\mathrm{Pr}\left(1 - \phi + \frac{(\rho Cp)_s}{(\rho Cp)_f}\phi\right)}{\left(\frac{k_s + 2k_f - 2\phi(k_f - k_s)}{k_s + 2k_f + \phi(k_f - k_s)}\right)}(1 - \eta^2 - \\ &7.72(\eta^2 - \eta^4) + 9.65(\eta^2 - \eta^6) - 8.19(\eta^2 - \eta^8) \\ &\quad + 4.02(\eta^2 - \eta^{10}) - 0.85(\eta^2 - \eta^{12}))1 + c_6(1 - \eta^2) + \\ &c_7(1 - \eta^4) + c_8(1 - \eta^6) + c_9(1 - \eta^8) + c_{10}(1 - \eta^{10}) \\ &\quad + \frac{4\alpha^2\,\mathrm{Pr}\,Ec}{\mathrm{Re}\left(\frac{k_s + 2k_f - 2\phi(k_f - k_s)}{k_s + 2k_f + \phi(k_f - k_s)}\right)(1-\phi)^{2.5}}(1 - \\ &\eta^2 - 7.72(\eta^2 - \eta^4) + 9.65(\eta^2 - \eta^6) - 8.19(\eta^2 - \eta^8) \\ &\quad + 4.02(\eta^2 - \eta^{10}) - 0.85(\eta^2 - \eta^{12}))^2 + \\ &0.041(-2\eta - 7.72(2\eta - 4\eta^3) - 8.19(2\eta - 6\eta^5) \\ &\quad -8.19(2\eta - 8\eta^7) + 4.02(2\eta - 10\eta^9) - \\ &0.85(2\eta - 12\eta^{11}))^2 \end{aligned} \tag{21}$$

By substituting the residual functions $R(c_1, c_2, c_3, c_4, c_5, \eta)$ and $R(c_6, c_7, c_8, c_9, c_{10}, \eta)$ into Eq. (17), a set of equation with four equations will appear and by solving this system of equations, coefficients $c_1 - c_{10}$ will be determined. For example, Using Galerkin method for a divergent channel with $Re = 100$, $Ec = 0.6$, $\phi = 0.04$ and $\alpha = 1°$, F($\eta$) and $\theta(\eta)$ are as follows:

$$\begin{aligned} &F(\eta) := 1 - 4.093594757\eta^2 + 7.723482110\eta^4 \\ &\quad -9.654433435\eta^6 + 8.194352902\eta^8 - \\ &4.021512058\eta^{10} + 0.8517052379\eta^{12} \end{aligned}$$

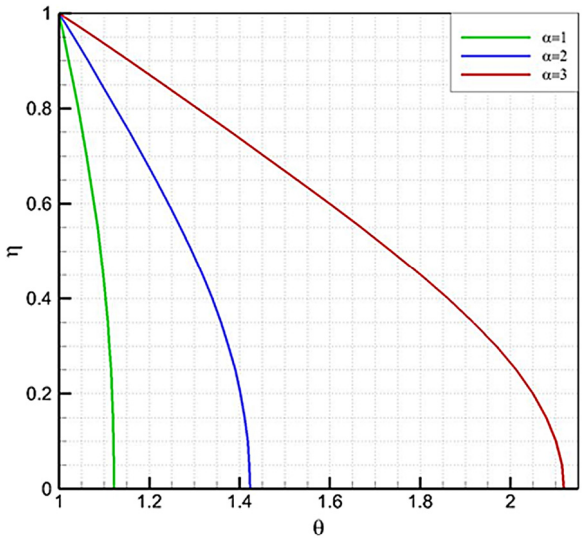


**Fig. 6.** Effect of the channel half angle on temperature profile when $Re = 50$, $Ec = 0.6$, $\phi = 0.04$ and $\Pr = 7$.

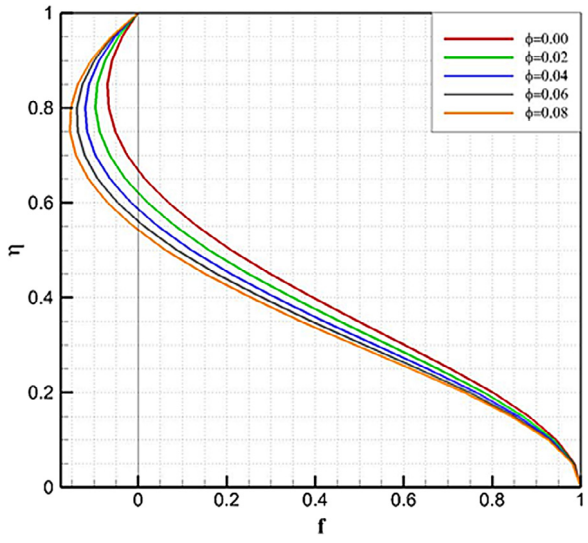


**Fig. 8.** Effect of the volume fraction of nanofluid on the velocity profile when $\alpha = 3$, $Re = 50$, $Ec = 0.6$ and $\Pr = 7$.

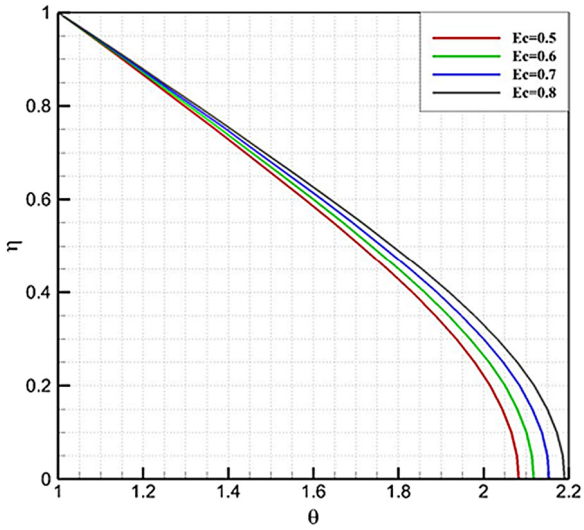


**Fig. 7.** Effect of the Eckert number on the temperature profile when $\alpha = 3$, $Re = 50$, $\phi = 0.04$ and $\Pr = 7$.

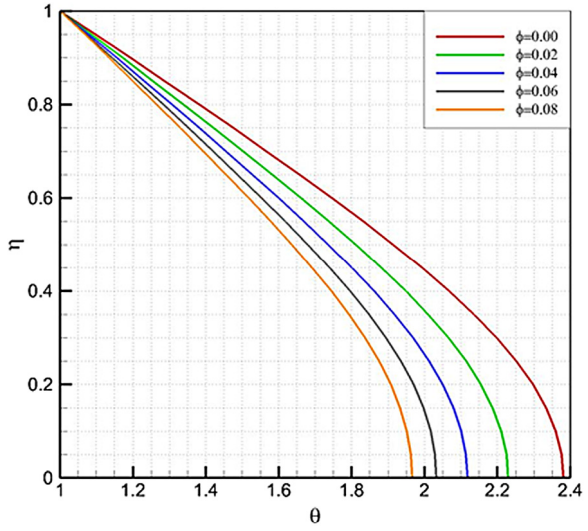


**Fig. 9.** Effect of the volume fraction of nanofluid on the temperature profile when $\alpha = 3$, $Re = 50$, $Ec = 0.6$ and $\Pr = 7$.

$$\theta(\eta) := 1.105274662 - 0.1062116884\eta^2 - 0.09738602812\eta^4 + 0.2364557276\eta^6 - 0.1998409456\eta^8 + 0.06170827150\eta^{10} \quad (22)$$

## 5. Results and discussions

In this paper flow and heat transfer between two diverging channel is investigated using Galerkin method (Fig. 1). Cu–water nanofluid is considered as working fluid.(See Table 1.) The numerical solution which is applied to solve the present case is the fourth order Runge–Kutta procedure. As shown in Fig. 2 and Table 2, GM has a good accuracy.

Effect of the Reynolds number on the velocity and temperature profiles are shown in Figs. 3 and 4. As Reynolds number increases both velocity and thermal boundary layer thicknesses decrease. Also it can be seen that back flow is stronger for higher Reynolds number. Effect of the channel half angle on the velocity and temperature profiles are shown in Figs. 5 and 6. Back flow is observed for higher values of angle. Increasing this angle makes thermal boundary layer thickness to increase so Nusselt number decreases with increase of this parameter. Effect of the Eckert number on the temperature profile is shown in Fig. 7. As Eckert number increase, viscous dissipation increase and in turn thermal boundary layer thickness decreases. Effects of the volume fraction of nanofluid on the velocity and temperature profile are shown in Figs. 8 and 9. As nanofluid volume fraction increases velocity increases. Also thermal boundary layer thickness decreases with increase of nanofluid volume fraction. So, rate of heat transfer increases with increase of nanofluid volume fraction.

## 6. Conclusion

In this paper, Galerkin method is used to solve the problem of Jeffery–Hamel nanofluid flow and heat transfer. It can be found

**Table 1**
Thermo physical properties of nanofluids and nanoparticles.

| | $\rho$ (kg/m$^3$) | $C_p$ (j/kg k) | k (W/m k) | $\beta \times 10^5$ (K$^{-1}$) | $\sigma$ ($\Omega$ m)$^{-1}$ |
|---|---|---|---|---|---|
| Pure water | 997.1 | 4179 | 0.613 | 21 | 0.05 |
| Copper (Cu) | 8933 | 385 | 401 | 1.67 | $5.96 \times 10^7$ |

**Table 2**
Comparison between numerical and applied methods for a divergent channel when Re = 100, $\phi = 0.04$ and $\alpha = 1°$ with Cu–water nanofluid.

| x | $F(\eta)$ | | $\theta(\eta)$ | |
|---|---|---|---|---|
| | GM | Nu | GM | Nu |
| 0 | 1 | 1 | 1.105275 | 1.105194 |
| 0.05 | 0.989814 | 0.989563 | 1.105009 | 1.104943 |
| 0.1 | 0.959827 | 0.958894 | 1.104203 | 1.104175 |
| 0.15 | 0.911696 | 0.90984 | 1.102838 | 1.102856 |
| 0.2 | 0.848016 | 0.845237 | 1.100885 | 1.100935 |
| 0.25 | 0.772084 | 0.768595 | 1.098311 | 1.098367 |
| 0.3 | 0.687613 | 0.683749 | 1.095086 | 1.095116 |
| 0.35 | 0.598425 | 0.594527 | 1.091194 | 1.091175 |
| 0.4 | 0.508164 | 0.504477 | 1.086632 | 1.086558 |
| 0.45 | 0.420058 | 0.416687 | 1.081422 | 1.081305 |
| 0.5 | 0.336758 | 0.333683 | 1.075609 | 1.075478 |
| 0.55 | 0.260274 | 0.257421 | 1.069262 | 1.069146 |
| 0.6 | 0.192003 | 0.189321 | 1.062466 | 1.062387 |
| 0.65 | 0.132832 | 0.130346 | 1.055312 | 1.055274 |
| 0.7 | 0.083291 | 0.081098 | 1.04789 | 1.047877 |
| 0.75 | 0.043703 | 0.041915 | 1.040269 | 1.040255 |
| 0.8 | 0.014292 | 0.012957 | 1.032493 | 1.032454 |
| 0.85 | −0.00478 | −0.00572 | 1.024574 | 1.024511 |
| 0.9 | −0.01346 | −0.0141 | 1.016502 | 1.016449 |
| 0.95 | −0.01184 | −0.0122 | 1.008282 | 1.008279 |
| 1 | 0 | 0 | 1 | 1 |

that GM has good accuracy. Results indicate that velocity boundary layer thickness decrease with increase of Reynolds number and nanoparticle volume friction. Thus skin friction coefficient has direct relationship with Reynolds number, opening angle and nanoparticle volume friction. Also it can be found that Nusselt number increases with increase of Reynolds number and nanoparticle volume friction.

## Acknowledgments

This research was supported by the National Sciences Foundation of China (NSFC) (No. U1610109), Yingcai Project of CUMT ( YC2017001), PAPD and UOW Vice-Chancellor's Postdoctoral Research Fellowship

## References

Ahmed, Naveed, Adnan, Khan, Umar, Mohyud-Din, Syed Tauseef, 2017. Unsteady radiative flow of chemically reacting fluid over a convectively heated stretchable surface with cross-diffusion gradients. Int. J. Therm. Sci. 121, 182–191.

Ali, Farhad, Ahmad Sheikh, Nadeem, Saqib, Muhammad, Khan, Arshad, 2017. Hidden phenomena of an MHD unsteady flow in porous medium with heat transfer. J. Nonlinear Sci. 101–116.

Ali, Farhad, Saqib, Muhammad, Khan, Ilyas, Ahmad Sheikh, Nadeem, 2016a. Application of Caputo-Fabrizio derivatives to MHD free convection flow of generalized Walters'-B fluid model. Eur. Phys. J. Plus 131 (10), 377.

Ali, Farhad, Jan, Syed AftabAlam, Khan, Ilyas, MadehaGohar, Sheik Ahmadh, Nadeem, 2016b. Solutions with special functions for time fractional free convection flow of brinkman-type fluid. Eur. Phys. J. Plus 131 (9), 310.

Abro, Kashif Ali, Khan, Ilyas, 2017. Analysis of the heat and mass transfer in the MHD flow of a generalized Casson fluid in a porous space via non-integer order derivatives without a singular kernel. Chinese J. Phys. 55, 1583–1595.

Aziz, A., Bouaziz, M.N., 2011. A least squares method for a longitudinal fin with temperature dependent internal heat generation and thermal conductivity. Energy Convers. Manage. 52, 2876–2882.

Bansal, L., 1994. Magnetofluiddynamics of Viscous Fluids. Jaipur Publishing House, Jaipur, India, OCLC 70267818.

Bouaziz, M.N., Aziz, A., 2010. Simple and accurate solution for convective-radiative fin with temperature dependent thermal conductivity using double optimal linearization. Energy Convers. Manage. 51, 76–82.

Cha, J.E., Ahn, Y.C., Kim, Moo-Hwan, 2002. Flow measurement with an electromagnetic flowmeter in two-phase bubbly and slug flow regimes. Flow Meas. Instrum. 12 (5–6), 329–339.

Chamkha, Ali J., Ahmed, S.E., 2011. Unsteady MHD stagnation-point flow with heat and mass transfer for a three-dimensional porous body in the presence of heat generation/absorption and chemical reaction. Prog. Comput. Fluid Dyn. 11 (6), 388–396.

Chamkha, Ali J., Abd El-Aziz, M.M., Ahmed, S.E., 2010. Effects of thermal stratification on flow and heat transfer due to a stretching cylinder with uniform suction/injection. Int. J. Energy Technol. 2 (4), 1–7.

Fengrui, Sun, Yuedong, Yao, Xiangfang, Li, Pengliang, Yu, Guanyang, Ding, Ming, Zou, 2017a. The flow and heat transfer characteristics of superheated steam in offshore wells and analysis of superheated steam performance. Comput. Chem. Eng. 100, 80–93.

Fengrui, Sun, Yuedong, Yao, Mingqiang, Chen, Xiangfang, Li, Lin, Zhao, Ye, Meng, Zheng, Sun, Tao, Zhang, Dong, Feng, 2017b. Performance analysis of superheated steam injection for heavy oil recovery and modeling of wellbore heat efficiency. Energy 125, 795–804.

Hamel, G., 1916. Spiralförmige Bewgungen Zäher Flüssigkeiten. Jahresber. Dtsch. Math.-Ver. 25, 34–60.

Hendi, F.A., Albugami, A.M., 2010. Numerical solution for Fredholm–Volterra integral equation of the second kind by using collocation and Galerkin methods. J. King Saud Univ., Eng. Sci. 22, 37–40.

Hosseini, S.R., Sheikholeslami, M., Ghasemian, M., Ganji, D.D., 2018. Nanofluid heat transfer analysis in a microchannel heat sink (MCHS) under the effect of magnetic field by means of KKL model. Powder Technol. 324, 36–47.

Imran, M.A., Khan, I., Ahmad, M., Shah, N.A., Nazar, M., 2017. Heat and mass transport of differential type fluid with non-integer order time-fractional Caputo derivatives. J. Molecular Liquids 229, 67–75.

Jafaryar, M., Sheikholeslami, M., Li, Zhixiong, Moradi, R., 2018. Nanofluid turbulent flow in a pipe under the effect of twisted tape with alternate axis. J. Therm. Anal. Calorim. http://dx.doi.org/10.1007/s10973-018-7093-2.

Khan, Umar, Adnan, Ahmed, Naveed, Mohyud-Din, Syed Tauseef, 2017. Heat transfer enhancement in hydromagnetic dissipative flow past a moving wedge suspended by H2O-aluminum alloy nanoparticles in the presence of thermal radiation. Int. J. Hydrogen Energy 42 (39), 24634–24644.

Mansour, M.A., Mohamed, R.A., Abd-ElAziz, M.M., Ahmed, S.E., 2010. Natural convection heat and mass transfer in porous triangular enclosures with the effects of thin fin and various thermal and concentration boundary conditions in the presence of heat source. Int. J. Energy Technol. 2 (3), 1–13.

Raju, C.S.K., Sandeep, N., 2016. Falkner Skan flow of a magnetic Carreau fluid past a wedge in the presence of cross diffusion. Eur. Phys. J. Plus 131, 267.

Shah, Z., Islam, S., Gul, T., Bonyah, E., Khan, M.A., 2018. The electrical MHD and hall current impact on micropolar nanofluid flow between rotating parallel plates. Results Phys. 9, 1201–1214.

Shaoqin, G., Huoyuan, D., 2008. negative norm least-squares methods for the incompressible magneto-hydrodynamic equations. Acta Math. Sci. B 28 (3), 675–684.

Sheikholeslami, M., 2017a. Influence of magnetic field on nanofluid free convection in an open porous cavity by means of Lattice Boltzmann Method. J. Molecular Liquids 234, 364–374.

Sheikholeslami, Mohsen, 2017b. Lattice Boltzmann method simulation of MHD non-Darcy nanofluid free convection. Physica B 516, 55–71.

Sheikholeslami, Mohsen, 2017c. Magnetic field influence on CuO -H2O nanofluid convective flow in a permeable cavity considering various shapes for nanoparticles. Int. J. Hydrogen Energy 42, 19611–19621.

Sheikholeslami, Mohsen, 2018a. CuO-water nanofluid flow due to magnetic field inside a porous media considering Brownian motion. J. Molecular Liquids 249, 921–929.

Sheikholeslami, M., 2018b. Numerical investigation for CuO-H2O nanofluid flow in a porous channel with magnetic field using mesoscopic method. J. Molecular Liquids 249, 739–746.

Sheikholeslami, M., 2018c. Numerical investigation of nanofluid free convection under the influence of electric field in a porous enclosure. J. Molecular Liquids 249, 1212–1221.

Sheikholeslami, M., 2018d. Numerical modeling of Nano enhanced PCM solidification in an enclosure with metallic fin. J. Molecular Liquids 259, 424–438.

Sheikholeslami, Mohsen, 2018e. Numerical simulation for solidification in a LHTESS by means of nano-enhanced PCM. J. Taiwan Inst. Chem. Eng. 86, 25–41.

Sheikholeslami, M., Bhatti, M.M., 2017. Forced convection of nanofluid in presence of constant magnetic field considering shape effects of nanoparticles. Int. J. Heat Mass Transfer 111, 1039–1049.

Sheikholeslami, M., Ghasemi, A., 2018. Solidification heat transfer of nanofluid in existence of thermal radiation by means of FEM. Int. J. Heat Mass Transfer 123, 418–431.
Sheikholeslami, M., Rokni, Houman B., 2017a. Nanofluid convective heat transfer intensification in a porous circular cylinder. Chem. Eng. Process.: Process Intensification 120, 93–104.
Sheikholeslami, M., Rokni, Houman B., 2017b. Simulation of nanofluid heat transfer in presence of magnetic field: A review. Int. J. Heat Mass Transfer 115, 1203–1233.
Sheikholeslami, Mohsen, Rokni, Houman B., 2017c. Melting heat transfer influence on nanofluid flow inside a cavity in existence of magnetic field. Int. J. Heat Mass Transfer 114, 517–526.
Sheikholeslami, M., Rokni, Houman B., 2018a. Magnetic nanofluid flow and convective heat transfer in a porous cavity considering Brownian motion effects. Phys. Fluids 30 (1). http://dx.doi.org/10.1063/1.5012517.
Sheikholeslami, M., Rokni, Houman B., 2018b. Numerical simulation for impact of Coulomb force on nanofluid heat transfer in a porous enclosure in presence of thermal radiation. Int. J. Heat Mass Transfer 118, 823–831.
Sheikholeslami, M., Rokni, Houman B., 2018c. CVFEM for effect of Lorentz forces on nanofluid flow in a porous complex shaped enclosure by means of Non-equilibrium model. J. Molecular Liquids 254, 446–462.
Sheikholeslami, Mohsen, Sadoughi, Mohammadkazem, 2017. Mesoscopic method for mhd nanofluid flow inside a porous cavity considering various shapes of nanoparticles. Int. J. Heat Mass Transfer 113, 106–114.
Sheikholeslami, Mohsen, Sadoughi, M.K., 2018. Simulation of CuO- water nanofluid heat transfer enhancement in presence of melting surface. Int. J. Heat Mass Transfer 116, 909–919.
Sheikholeslami, M., Seyednezhad, M., 2017a. Lattice Boltzmann Method simulation for CuO-water nanofluid flow in a porous enclosure with hot obstacle. J. Molecular Liquids 243, 249–256.
Sheikholeslami, M., Seyednezhad, M., 2017b. Nanofluid heat transfer in a permeable enclosure in presence of variable magnetic field by means of CVFEM. Int. J. Heat Mass Transfer 114, 1169–1180.
Sheikholeslami, Mohsen, Seyednezhad, Mohadeseh, 2018. Simulation of nanofluid flow and natural convection in a porous media under the influence of electric field using CVFEM. Int. J. Heat Mass Transfer 120, 772–781.
Sheikholeslami, M., Shehzad, S.A., 2017a. CVFEM for influence of external magnetic source on Fe3O4 –H2O nanofluid behavior in a permeable cavity considering shape effect. Int. J. Heat Mass Transfer 115, 180–191.
Sheikholeslami, M., Shehzad, S.A., 2017b. Magnetohydrodynamic nanofluid convective flow in a porous enclosure by means of LBM. Int. J. Heat Mass Transfer 113, 796–805.
Sheikholeslami, M., Shehzad, S.A., 2018a. CVFEM simulation for nanofluid migration in a porous medium using Darcy model. Int. J. Heat Mass Transfer 122, 1264–1271.
Sheikholeslami, M., Shehzad, S.A., 2018b. Numerical analysis of Fe3O4 –H2O nanofluid flow in permeable media under the effect of external magnetic source. Int. J. Heat Mass Transfer 118, 182–192.
Sheikholeslami, M., Shehzad, S.A., 2018c. Simulation of water based nanofluid convective flow inside a porous enclosure via Non-equilibrium model. Int. J. Heat Mass Transfer 120, 1200–1212.
Sheikholeslami, M., Zeeshan, A., 2017. Mesoscopic simulation of CuO-H2O nanofluid in a porous enclosure with elliptic heat source. Int. J. Hydrogen Energy 42 (22), 15393–15402.
Sheikholeslami, M., Darzi, Milad, Li, Zhixiong, 2018a. Experimental investigation for entropy generation and exergy loss of nano-refrigerant condensation process. Int. J. Heat Mass Transfer 125, 1087–1095.
Sheikholeslami, M., Darzi, Milad, Sadoughi, M.K., 2018b. Heat transfer improvement and pressure drop during condensation of refrigerant-based nanofluid; An experimental procedure. Int. J. Heat Mass Transfer 122, 643–650.
Sheikholeslami, M., Hayat, T., Alsaedi, A., 2017. On simulation of nanofluid radiation and natural convection in an enclosure with elliptical cylinders. Int. J. Heat Mass Transfer 115, 981–991.
Sheikholeslami, M., Hayat, T., Alsaedi, A., 2018c. Numerical simulation for forced convection flow of MHD CuO-H2O nanofluid inside a cavity by means of LBM. J. Molecular Liquids 249, 941–948.
Sheikholeslami, M., Jafaryar, M., Li, Zhixiong, 2018d. Nanofluid turbulent convective flow in a circular duct with helical turbulators considering cuo nanoparticles. Int. J. Heat Mass Transfer 124, 980–989.
Sheikholeslami, M., Ganji, D.D., Ashorynejad, H.R., Rokni, H.B., 2012. Analytical investigation of Jeffery–Hamel flow with high magnetic field and nanoparticle by Adomian decomposition method. Appl. Math. Mech. -Engl. Ed. 33 (1), 25–36.
Sheikholeslami, Mohsen, Hayat, Tasawar, Muhammad, Taseer, Alsaedi, Ahmed, 2018e. MHD forced convection flow of nanofluid in a porous cavity with hot elliptic obstacle by means of Lattice Boltzmann method. Int. J. Mech. Sci. 135, 532–540.
Sheikholeslami, M., Jafaryar, M., Ganji, D.D., Li, Zhixiong, 2018f. Exergy loss analysis for nanofluid forced convection heat transfer in a pipe with modified turbulators. J. Molecular Liquids 262, 104–110.
Sheikholeslami, M., Shehzad, S.A., Li, Zhixiong, 2018g. Water based nanofluid free convection heat transfer in a three dimensional porous cavity with hot sphere obstacle in existence of lorenz forces. Int. J. Heat Mass Transfer 125, 375–386.
Ullah, Imran, Shafie, Sharidan, Khan, Ilyas, 2017. Effects of slip condition and Newtonian heating on MHD flow of Casson fluid over a nonlinearly stretching sheet saturated in a porous medium. J. King Saud Univ., Eng. Sci. 29, 250–259.
Vaferi, B., Salimi, V., Dehghan Baniani, D., Jahanmiri, A., Khedri, S., 2012. Prediction of transient pressure response in the petroleum reservoirs using orthogonal collocation. J. Petrol. Sci. Eng. http://dx.doi.org/10.1016/j.petrol.2012.04.023.
Zin, Nor Athirah Mohd, Khan, Ilyas, Shafie, Sharidan, Alshomrani, Ali Saleh, 2017. Analysis of heat transfer for unsteady MHD free convection flow of rotating Jeffrey nanofluid saturated in a porous medium. Results Phys. 7, 288–309.